

Rotational Excitation Dynamical Model and Micro-vibration Characteristics of Momentum Wheel



Yanhong Ma, Shanshan Liu, Hong Wang, and Jie Hong

Abstract The momentum wheel is a critical component of high-precision stable platform of the spacecraft. During the working process, with the continuous improvement of satellite performances such as attitude stability and imaging precision, the influence of micro-vibration on the control accuracy of the momentum wheel becomes increasingly prominent. In order to improve the attitude control accuracy of the spacecraft, it is necessary to suppress the disturbance force (moment) from momentum wheel. Based on the structural and mechanical characteristics of the components, the rotational excitation dynamical model of the momentum wheel is established, and the vibration sources of micro-vibrations are obtained. Hereby a finite element model of the momentum wheel with structural and excitation characteristics will also be established. Combined with the test of modal vibration characteristics and the waterfall diagram of the ascent, the results show that the non-uniform and non-continuity of wheel body is the main reason for the low-order traveling-wave vibration of the momentum wheel during operation; the asymmetry of the strut structure and the bearing support structure leads to the harmonic excitation vibration.

Keywords Momentum wheel · Micro-vibration · Non-uniformity · Traveling wave vibration · Harmonic-wave excitation

Y. Ma · S. Liu · J. Hong (✉)

School of Energy and Power Engineering, Beihang University, Beijing 100083, China
e-mail: hongjie@buaa.edu.cn

Y. Ma

e-mail: mayanhong@buaa.edu.cn

S. Liu

e-mail: liushanshan633@buaa.edu.cn

Y. Ma · J. Hong

Collaborative Innovation Center of Advanced Aero-Engine, Beijing 100083, China

H. Wang

Beijing Key Laboratory of Long-Life Technology of Precision Rotation and Transmission Mechanism, Beijing Institute of Control Engineering, Beijing 100094, China
e-mail: wangh1981@sina.com

© Springer Nature Singapore Pte Ltd. 2021

E. J. Sapountzakis et al. (eds.), *Proceedings of the 14th International Conference on Vibration Problems*, Lecture Notes in Mechanical Engineering, https://doi.org/10.1007/978-981-15-8049-9_41

1 Introduction

The momentum wheel becomes its own excitation source due to its structural characteristics during the ascent or at one certain speed rotation, so that the output moment load contains wide-frequency micro-amplitude vibration, which is called “micro-vibration”. Because of its small amplitude and high frequency, it will not have a significant impact on most spacecraft, but the high-precision torque control momentum wheel will seriously affect the important performance indicators such as accuracy, stability, and resolution of the payload [1].

The research on the micro-vibration of the momentum wheel mainly includes three aspects: theoretical analysis, experimental verification, and simulation modal. The related research of theoretical analysis began in 1970s. Hasha [2] considered that the disturbance is a series of discrete resonances proportional to the square of the rotating speed of the momentum wheel. The coefficient of the empirical model is determined according to the test results, but the inertia moment of the rotor and disturbance of the bearing is not considered. Masterson [3] derived the relationship between the unbalance and disturbance, and established the fundamental frequency resonance analytical model, but could not explain the backward precession. Liu [4] introduced the broadband noise into the disturbance, and obtained the vibration mode and the forward/backward precession at low speed, but could not explain the high frequency and high-order vibration of the system.

Related tests mainly include ground micro-vibration test, test of micro-vibration disturbance source, micro-vibration isolation test, etc. Yang et al. [5] studied the micro-vibration characteristics at different rotating speeds through ground micro-vibration test and summarized the transfer characteristics and the influence of satellite boundary conditions on the waterfall map. NASA and the German Space Agency [6] conducted two in-orbit micro-vibration dynamic environment experiments, namely, IPEX experiments, which were mainly concerned with on-track mechanical disturbances and thermal disturbances, they had finished modeling, verification, and structural design for high-frequency disturbances.

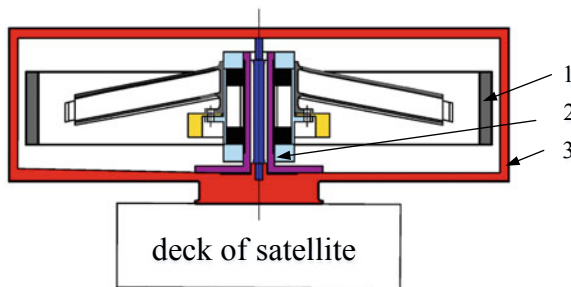
Simulation models mainly include that Zhou [7] established the momentum wheel vibration equation based on the linear assumption, but he only considered the static unbalance of the wheel body while the dynamic imbalance, the gyro effect and the bearing rolling effect were not considered. The result is that only vibration amplitude of the fundamental harmonic has been calculated. Luo et al. [8] proposed a bearing compaction excitation model. They analyzed the non-linear contact of the bearing rolling surface geometric error as the disturbance source, thus carried out the corresponding experimental verification, but lacked the mechanism analysis of the excitation from the momentum wheel self. Li et al. [9] used the Jeffcott rotor model to propose exciting forces from unbalance and elastic vibration inside the rotor system, similarly the effects of support misalignment and roller excitation were not considered.

In summary, in the existing theoretical models and simulation calculations, the momentum wheel is mostly assumed to be a continuous stable structure. The vibration

characteristics of the structural system under excitation such as unbalance are studied, but the incentives coming from connection interface and its change of the momentum wheel in the rotating state is less concerned. The relevant experimental research pays more attention to the vibration response amplitude and ignores the influence of the inherent vibration characteristics of the structure. Therefore, the vibration damping and vibration isolation design of the momentum wheel is not targeted. Only by comprehensively considering the vibration generating mechanism in different frequency domains can the momentum wheel micro-vibration be more effectively suppressed. Based on the structural and mechanical characteristics of the components of the momentum wheel, this paper establishes a rotational excitation dynamical model of the momentum wheel, and then explains the vibration source of micro-vibration, then the paper uses the finite element model with structural and excitation characteristics equivalent to verify the source of traveling wave vibration and high harmonic-wave vibration combined with the corresponding test.

2 Structural Characteristics and Dynamical Model of the Momentum Wheel

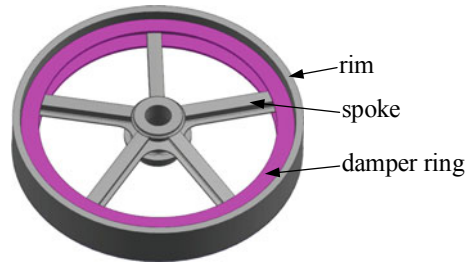
The simplified schematic graph of the momentum wheel structural system is shown in Fig. 1. It mainly includes five parts: the wheel structure, the bearing support structure, and the shell structure.



(1-the wheel structure; 2-the bearing support structure; 3-the shell structure)

Fig. 1 Simplified schematic graph of the momentum wheel structural system

Fig. 2 Schematic diagram of the wheel structure



2.1 Structural Characteristics

2.1.1 The Wheel Structure

The wheel body is combined into a main structure by shell-shaped rim and beam-shaped spokes and is equipped with a double annular damper rings adopting with bolt connection. This geometry makes the wheel structure non-continuous and its mass/stiffness distribution non-uniform, as shown in Fig. 2.

The shell-shaped rim and the beam-shaped spokes constituting the wheel structure can reduce its weight while providing a large moment of inertia and realize the storage and release of kinetic energy by adjusting the angular velocity. The rim of the large-diameter and thin-wall structure will produce traveling wave vibration at high speed rotating [10].

The double annular damper rings are also the main components of the wheel structure. The damper ring is overlapped with the rim and the spoke, and the bolt fixing structure is adopted. In operation, the damper rings reduce the vibration-damping force of the momentum wheel output by absorbing the vibration energy of the wheel body self and the energy of interface contact friction. However, the natural vibration frequency's minor changes of the damper rings during the rotation and the constraint characteristics of the fixing bolts also affect the vibration characteristics of the wheel structure.

2.1.2 The Bearing Support Structure

The bearing support structure includes two pairs of bearings and a strut. The bearing consists of non-continuous structures such as rollers, inner/outer rings, and a bearing retainer. The rolling contact between rollers and inner/outer rings is volatility and periodicity. On the one hand, it causes (secondary) doubling frequency excitation, and on the other hand, the support stiffness is time-varying [11]. The outer ring of the bearing is connected to the rotating wheel body, while the inner ring does not rotate. Two pairs of diagonal contact ball bearings are located on both sides of the wheel body, as shown in Fig. 3.

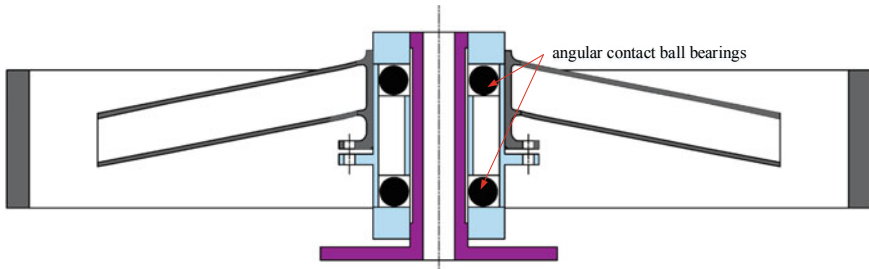


Fig. 3 Schematic diagram of bearing support structure

The vibration load of the wheel body is transmitted to the outer ring and then transmitted to the inner ring via the rollers. The axial load can be borne by all rollers, while the radial load is borne by partial rollers within one sector.

According to the Hertz contact elastic theory and the boundary conditions of the balance of force, it is known as

$$F_r = zQ_{\max} \frac{1}{2\pi} \int_{-\phi}^{\phi} (\cos \varphi)^{\frac{5}{2}} d\varphi \tag{1}$$

where F_r is the radial load; z is the total number of rollers; φ is the angle between the load line and the line of bearings shaft; Φ is the half angle of the maximum force sector; Q_{\max} is the maximum radial force on the rollers [12]. As shown in Fig. 4, (a) and (b) are two forms of “odd” rolling and “even” rolling appearing in the roller-inner/outer rings at intervals of time π/Ω . The rotating speed of the bearing is Ω , and the rotating speed of the rollers is ω_r . Supposing the radial load of the outer ring at

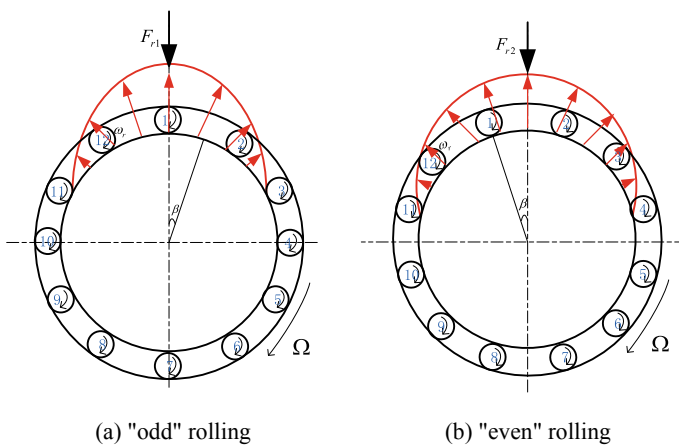


Fig. 4 Schematic graph of loads on rollers

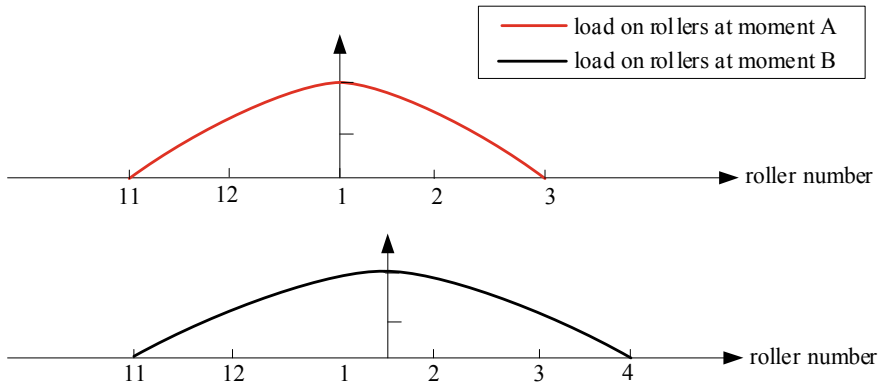


Fig. 5 Force on the rollers at two moments

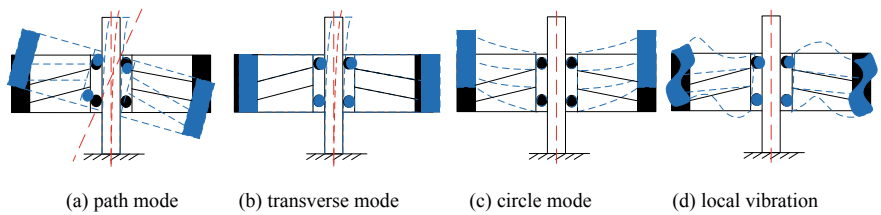


Fig. 6 Schematic diagram of typical mode shape

time A is the simple harmonic force of the amplitude $F_{r1} = F \sin \omega t$, there are three rollers in the figure being stressed; the radial load of the outer ring at time B becomes $F_{r2} = F \sin(\omega t + \beta)$, and there are four rollers being stressed. It can be known from Eq. (1) that the two moments are different, so the load transmitted to the inner ring of the bearing is also different. Therefore, the force on the rollers at two moments is shown as Fig. 5. It can be seen that when a certain point of outer ring is bearing harmonic force, it will cause the harmonic force of different amplitudes on multiple rollers. As the roller rotates and revolves, it will eventually induce traveling wave excitation to the inner ring. In addition, each structural component of the bearing has its own natural vibration frequency, only if the excitation frequency is close to the natural frequency, it will also excite the resonance of that component.

The geometric feature of the strut structure is an elongated cantilever beam with a large flange. The slender beam will vibrate together with the wheel body, so that the bearings which are symmetric with respect to the wheel body exhibit incomplete symmetry of rigidity, that is, the support is misaligned (parallel and angular misalignment). This situation is the main reason for the secondary frequency excitation of unbalance disturbance force.

As shown in Fig. 6, due to the joint action of the bearing and strut, the four typical mode shapes of the wheel are path mode, transverse mode, circle mode and local vibration [13].

2.2 Dynamical Model of the Momentum Wheel Structural System

The dynamical model of the momentum wheel structural system is shown in Fig. 7. The wheel is simplified to a body in the form of rim-spokes; the bearing is simplified to two pairs of linear spring units of different radial stiffness. OXYZ is a fixed coordinate system and at the bottom of the pole; $O_1X_1Y_1Z_1$ is a local coordinate system, and its center is the mass center of the wheel, O_1X_1 and O_1Y_1 are the two principal axes of inertia. The transformation matrix between two coordinate systems can be shown in Table 1.

Where $(x_0, y_0, z_0, 0, 0)^T$ is the coordinate of the mass center of the wheel in fixed coordinate system, and γ is the angle of $O_1X_1Y_1Z_1$ relative to OXYZ. Therefore, the coordinate conversion of the two coordinate systems is $q = Rq_1 + S$.

According to the Lagrange equation, the kinetic energy of the system includes the translational kinetic energy and rotational kinetic energy of the wheel structure;

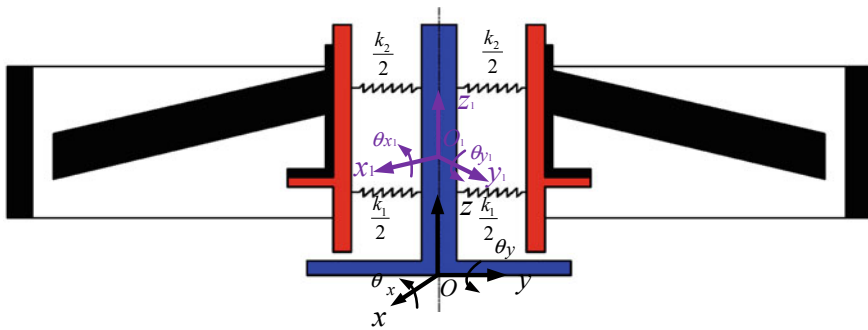


Fig. 7 Dynamical model of the momentum wheel structural system

Table 1 Transformation matrix between two coordinate systems

Translation	Rotation
$S = \begin{Bmatrix} x_0 \\ y_0 \\ z_0 \\ 0 \\ 0 \end{Bmatrix}$	$R = \begin{bmatrix} \cos \gamma & -\sin \gamma & 0 & 0 & 0 \\ \sin \gamma & \cos \gamma & 0 & 0 & 0 \\ 0 & 0 & 1 & 0 & 0 \\ 0 & 0 & 0 & 1 & 0 \\ 0 & 0 & 0 & 0 & 1 \end{bmatrix}$

the potential energy of the system includes the elastic potential energy of the wheel structure and the elastic potential energy of the two pairs of springs. Thus, the matrix form of the kinetic equation can be derived:

$$M\ddot{q} + G\dot{q} + Kq = Q \tag{2}$$

where q is generalized coordinates; \dot{q} is generalized speed, which is $q = \{x, y, z, \theta_x, \theta_y\}^T$; \ddot{q} is generalized acceleration; M is mass matrix; G is gyro matrix; K is stiffness matrix; Q is generalized excitation force vector.

The expression of M is

$$M = \begin{bmatrix} m & 0 & 0 & 0 & 0 \\ & m & 0 & 0 & 0 \\ & & m & 0 & 0 \\ & sym & & J_x & 0 \\ & & & & J_y \end{bmatrix} \tag{3}$$

Combined with the structural characteristics of the wheel structure, the influencing factors will be analyzed. On the one hand, the position of the mass center of the wheel changes slightly during the rotation process, which will affect the generalized displacement. On the other hand, with the elastic deformation of the wheel body, small changes will also occur, and they act together as a parameter excitation.

The expression of G is

$$G = \Omega \begin{bmatrix} 0 & 0 & 0 & 0 & 0 \\ 0 & 0 & 0 & 0 & 0 \\ 0 & 0 & 0 & 0 & 0 \\ 0 & 0 & 0 & 0 & J_p \\ 0 & 0 & 0 & -J_p & 0 \end{bmatrix} \tag{4}$$

As can be seen, G is a function of Ω , that is, its influence on the vibration response depends on the rotating speed.

K includes both the stiffness of the elastic deformation of the wheel and the stiffness of the support.

The main influencing factor of the former is the radial stiffness of the rim. The wheel body is composed of rims and spokes with different geometric configurations. Therefore, it is a rotationally symmetrical rather than an axisymmetric structure, and thus the stiffness/mass is unevenly distributed along the circumferential direction. As shown in Fig. 8, the angle between the normal of spoke and the centroid axis will lead the mass center of the wheel to a slight offset along the axial direction during high speed rotating.

The polar coordinate system is established where the angle between the rim micro-element and the center line of the spoke is the independent variable, as shown in Fig. 9, taking the ratio of the radial stiffness and local sectional area to express

Fig. 8 Schematic diagram of the angle and force of the spokes

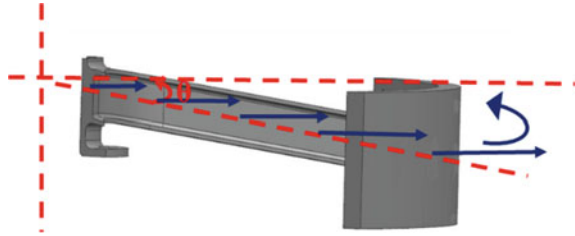
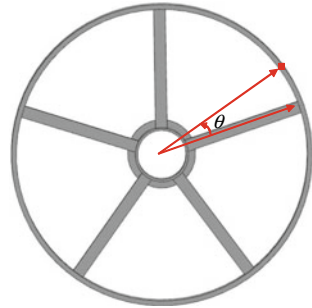


Fig. 9 Schematic diagram of the rim radial stiffness polar coordinate system



the stiffness/mass, and the variation with the circumferential angle is calculated. As shown in Fig. 10, the stiffness/mass of the momentum wheel is unevenly distributed along the circumferential direction, and the radial deformation is most likely to occur in the middle of the spoke, and the radial stiffness will be abrupt at the joint [14].

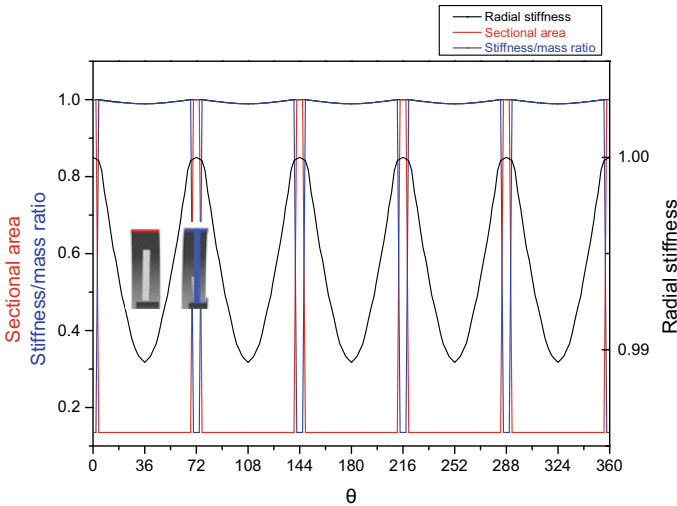
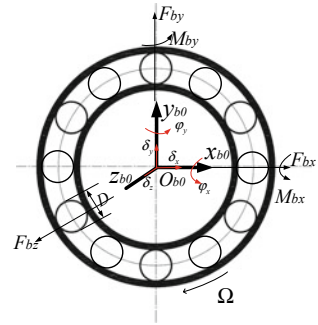


Fig. 10 Section stiffness/mass along the circumferential direction

Fig. 11 Bearing coordinate system and force diagram



Therefore, the stiffness is both a function of the circumferential angle and a function of the rotating speed, which forms a parameter excitation.

The influencing factor of the latter is mainly the bearing stiffness under the misalignment. As shown in Fig. 11, it is a bearing coordinate system and its force diagram. According to Newton’s mechanics and Hertz contact theory, considering the parallel and angular misalignment, the five degree of freedom (three translation degrees and two rotation degrees) stiffness model of the rolling bearing under the misalignment state is established. Bearing preload force is generated as F_{bz} . Parallel misalignment is equivalent to applying radial load (F_{bx} or F_{by}) to the bearing, angle misalignment is equivalent to applying a bending moment (M_{bx} or M_{by}) to the bearing. The expression of the bearing stiffness matrix \mathbf{K}_b can be written as

$$\begin{aligned}
 \mathbf{K}_b &= \mathbf{K}_{b0} + \Delta\mathbf{K}_{bp} + \Delta\mathbf{K}_{ba} = \begin{bmatrix} \frac{\partial F_{bx}}{\partial \delta_x} & 0 & 0 & 0 & 0 \\ & \frac{\partial F_{by}}{\partial \delta_y} & 0 & 0 & 0 \\ & & \frac{\partial F_{bz}}{\partial \delta_z} & 0 & 0 \\ sym & & & \frac{\partial M_{bx}}{\partial \phi_x} & 0 \\ & & & & \frac{\partial M_{by}}{\partial \phi_y} \end{bmatrix} \\
 &= \begin{bmatrix} K_{11} & 0 & 0 & 0 & 0 \\ & K_{22} & 0 & 0 & 0 \\ & & K_{33} & 0 & 0 \\ sym & & & K_{44} & 0 \\ & & & & K_{55} \end{bmatrix} \quad (5)
 \end{aligned}$$

where \mathbf{K}_{b0} is the stiffness matrix under normal installation conditions, $\Delta\mathbf{K}_{bp}$ is the additional stiffness matrix caused by parallel misalignment, and $\Delta\mathbf{K}_{ba}$ is the additional stiffness matrix caused by angular misalignment. It can be seen that when two pairs of bearings on the strut are subjected to different forces, the stiffness is also different [15]. So, this stiffness is time-varying, non-linear and is related to rotational deformation.

\mathbf{Q} is mainly from the unbalance excitation of the rotating process, and its frequency is the same as the rotating speed. Even a precise dynamic balance cannot

completely eliminate the imbalance. In addition, there are double-frequency and (secondary) harmonic excitations caused by bearing rollers. When the frequency of the harmonic excitation is the same as the natural frequency of the local vibration of some component, the local vibration response will be significantly higher than other frequencies occurs.

The disturbance force (moment) output from the bottom mount of the strut can be obtained by Laplace transforming the excitation force (moment) at the centroid of the wheel body [16]. In summary, the wheel structure has non-uniformity and non-continuity, which generates inertial load when rotating at high speed, causing parameter disturbance excitation of mass matrix M and stiffness matrix K ; the rolling action from bearing rollers and cantilever strut contributes to the traveling wave which becomes excitation characteristics arousing high-frequency excitation in Q .

3 Micro-vibration Characteristics Under Simulated Rotation

In order to verify the micro-vibration characteristics caused by the structural characteristics of the momentum wheel in the previous section, the finite element software is used to establish the model of the structural system. Then the inherent characteristics in the full speed range can be calculated, and the response characteristics can be calculated upon loading rotational excitation.

3.1 Model Establishment

The finite element model of the momentum wheel structural system is shown in Fig. 12, including the wheel body (rim-spoke connection structure), the damper rings and the strut. The bearings use combine 214 unit. All bodies are meshed by solid element. The bottom of the strut is fully constrained; between the damper ring and

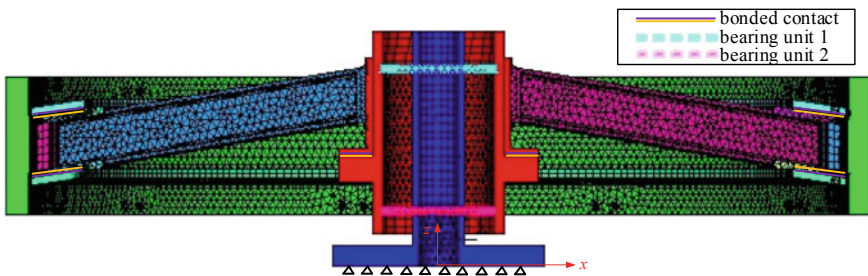


Fig. 12 Finite element model of the momentum wheel structural system

the spoke, bounded contact unit is used. Considering assembly error the connection between two damper rings is a spring unit, or some where are coordinated by radial and axial displacement.

3.2 Inherent Characteristic

Adding rotating speed loads on the rotor assembly (the wheel body and the damper rings), the inherent characteristics of the momentum wheel structural system is calculated, and the corresponding Campbell diagram is shown in Fig. 13. The first six-order modal characteristic is listed in Table 2, simultaneously extracting the radial deformation and the circumferential wave number of the rim in each step.

According to the traveling wave theory of the rotating case, the traveling wave frequencies of the rim are $\omega = \omega_d \pm \frac{m^2-1}{m^2+1}m\Omega$, where ω_d is the natural frequency of the rim rotation. When $m > 1$, the frequencies of forward and backward traveling waves are different, and there are “V” lines on the Campbell diagram. When $m = 1$, there is no traveling wave characteristic in theory, however, in the second order there is still a small bifurcation because of the gyro moment effect caused by bending of the strut.

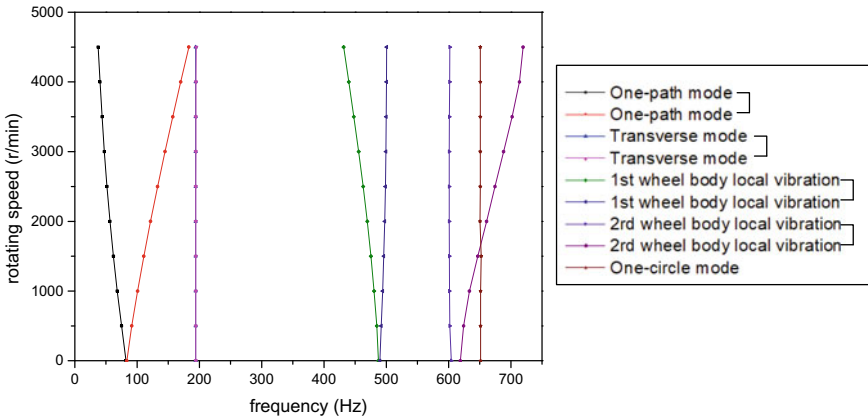
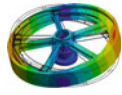
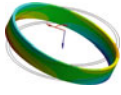
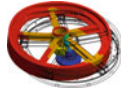
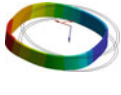
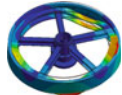
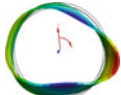
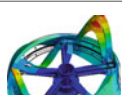
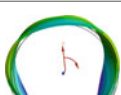
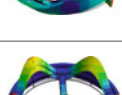
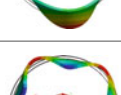


Fig. 13 Campbell diagram of the momentum wheel structural system

Table 2 Modal characteristics of each order

Order	Frequency (Hz)	Mode	Overall mode	Rim radial deformation
1	82	One-path mode		
2	194	Transverse mode		
3	487	1st wheel body local vibration		
4	604	2nd wheel body local vibration		
5	651	One-circle mode		

3.3 Response Characteristics

3.3.1 Harmonic-Wave Excitation

In order to simulate the double-frequency excitation under the action of bearings rolling action, the harmonic response is calculated by unbalance excitation. The frequencies are $1x$, $2x$, and $3x$ of the speed, respectively, and the displacement of a point at the fulcrum on the strut structure is calculated. By dimensionless processing, we can obtain three response rays starting from the origin, as shown in Fig. 14. It can be seen that the response tendency in three directions is basically the same, but the amplitude of Z-direction is much smaller than that in X- and Y-directions; the peak of the vibration response takes place at the intersection with the intrinsic characteristic line; the response amplitude of the base frequency excitation is substantially parabolic.

3.3.2 Traveling Wave Characteristics

For the four speeds (1000, 2000, 3000, 3000 r/min) in the process of speed increase, the load condition is set as the transient response under the unbalance, and the

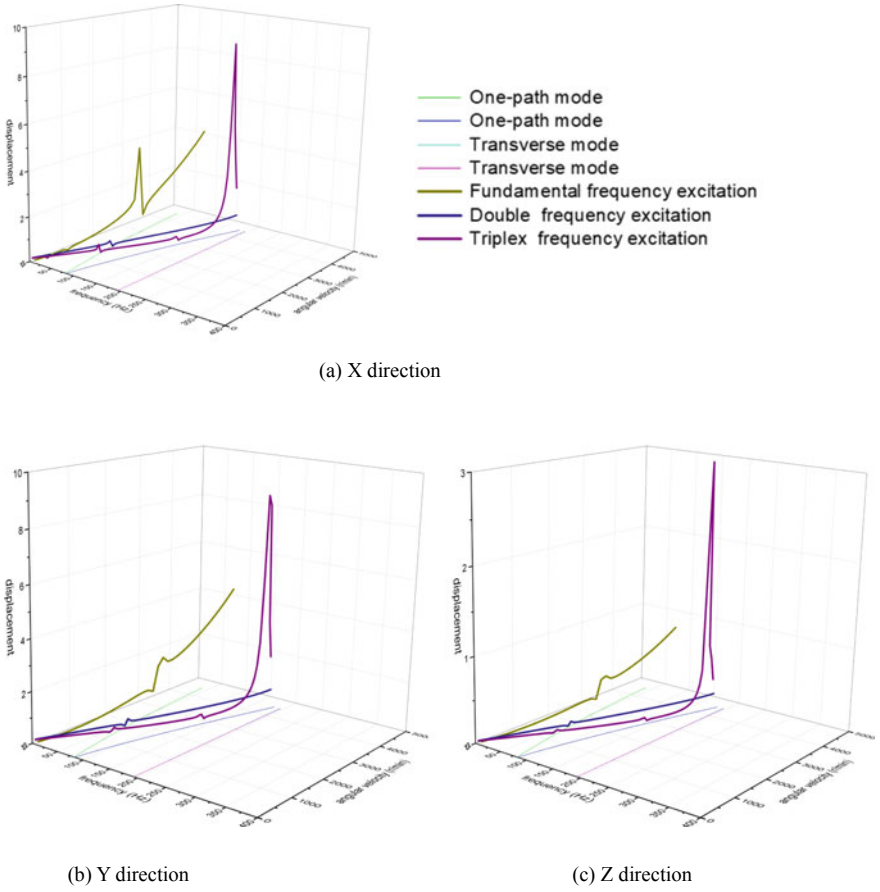


Fig. 14 Harmonic excitation response characteristics of the structural system

displacement of a point at the fulcrum on the strut structure is calculated, which should be in unstable period. The displacement response curve through FFT transformation changes to be a waterfall diagram in three directions as shown in Fig. 15. It can be seen from the figure that since the applied load is unbalance excitation, the response amplitude is maximum when the frequency is base frequency on each certain speed line; the peak frequency except the excitation frequency on each speed line is the natural frequency of the structure, and its value is related to the rotating speed, we can obtain the “V” shape line by connecting the corresponding points; when the frequency of the backward traveling wave is far from the excitation frequency, the response amplitude is the same as the magnitude of the forward wave, while when the frequency of the backward wave is close to the excitation frequency, the point will have a large response, such as the line with the speed of 3000r/min in each figure; with the rotation speed accelerates, the frequency of the one-path mode will

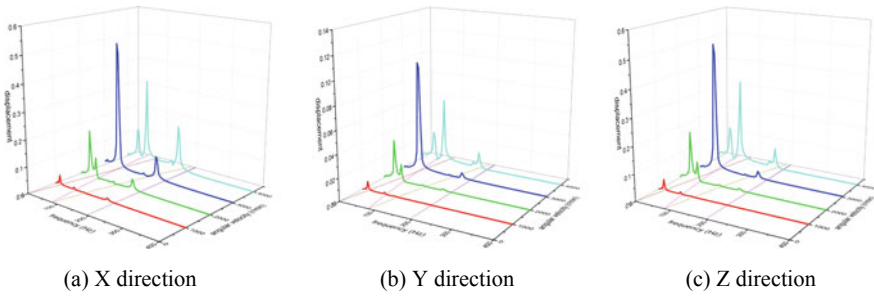


Fig. 15 Simulation waterfall diagram of the structural system

change, and then the traveling wave characteristics appear, however, the frequency of the transverse mode does not substantially change.

4 Vibration Characteristics Test

In this section, via the experiment, the natural mode of the momentum wheel structural system within 1000 Hz with no-speed is obtained, and the main modal mode generated by micro-vibration is analyzed. In the process of ascent, the waterfall diagram of the momentum wheel structural system is tested, the excitation source inside the structural system is analyzed, and the correctness of the theoretical model and simulation calculation is verified.

4.1 Inherent Modal Characteristics with No-Speed

The natural mode is the property of the structural system itself. When the excitation frequency is close to some certain mode, the vibration response is largely determined by the mode. The experiment tests the inherent modal characteristics of the momentum wheel structural system. Since the vibration mode of the system is mainly based on the deformation of the wheel structure, the measuring points are arranged on the wheel body and the upper damper ring, as shown in Fig. 16, the wheel body has 40 axial points and 30 radial points and the damper ring has 30 axial points. The modal frequency and mode shape were measured by the hammer of multi-point excitation and single-point pick-up. The test obtained the various modes of the axial deformation, radial deformation of the wheel and axial deformation of the damper ring within 1000 Hz, as shown in Table 3.

It can be seen from the table that the first, fourth, fifth, and sixth steps are all local vibration modes of the wheel body, which are caused by the structural characteristics of the wheel body itself. The second step is the transverse mode of the wheel along

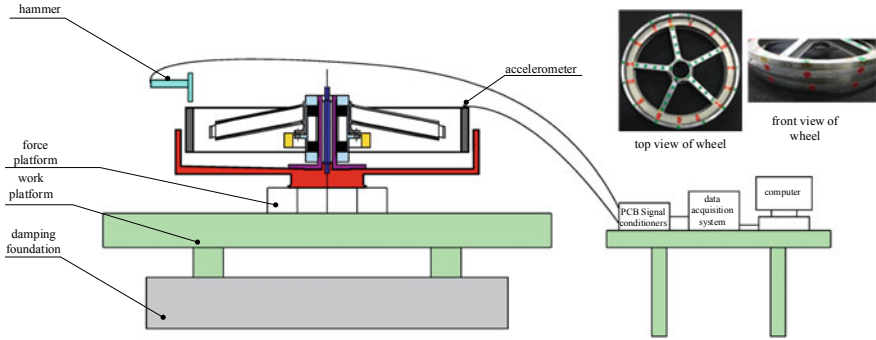


Fig. 16 Schematic diagram of the test device for the inherent modal characteristics of the momentum wheel structural system

Table 3 Test results of inherent modal characteristics

Order	Frequency (Hz)	Mode	Axial deformation of wheel	Radial deformation of wheel	Axial deformation of damper ring
1	86	One-path mode			
2	195	Transverse mode			
3	306	Damper ring local mode	Not obvious	Not obvious	
4	491	1st wheel body local vibration			
5	571	2nd wheel body local vibration			Not obvious
6	675	One-circle mode			Not obvious

with the strut. The third step is a local vibration of the damper ring that is inevitable due to assembly error.

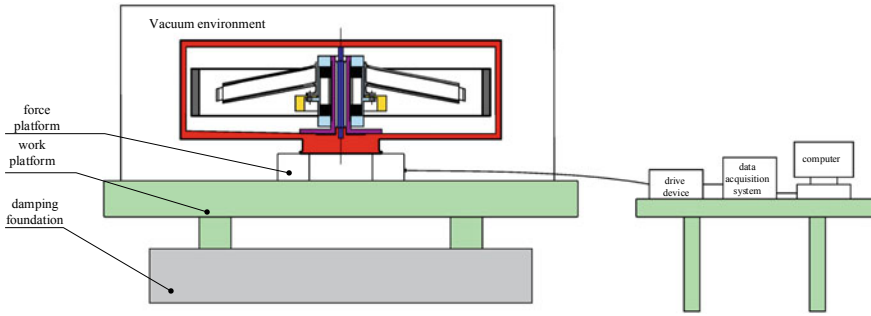
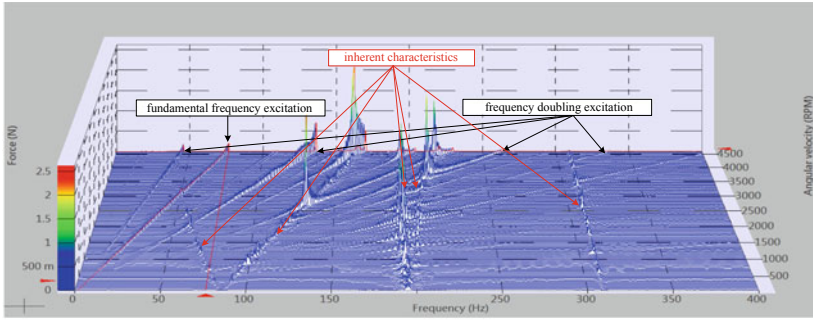


Fig. 17 Schematic diagram of the waterfall diagram test device of the momentum wheel structural system

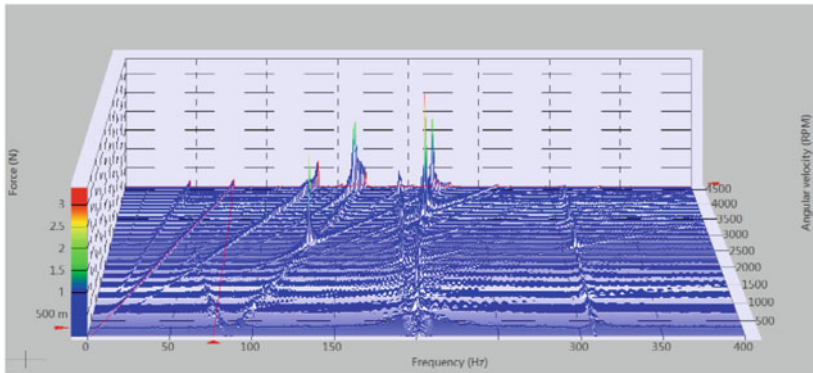
4.2 Waterfall Diagram of the Ascent Process

Under the action of rotation, the inherent characteristics of the momentum wheel structural system will change. The Kistler force measuring device was used to imitate the speed-up process of the momentum wheel under vacuum conditions, and the waterfall diagram of the disturbance output of the pedestal was obtained. A schematic diagram of the waterfall diagram test device is shown in Fig. 17, in which the wheel structure has been dynamically balanced. As shown in Fig. 18, it is the disturbance force waterfall diagram in three directions within 400 Hz (the coordinate system is the same as Fig. 7).

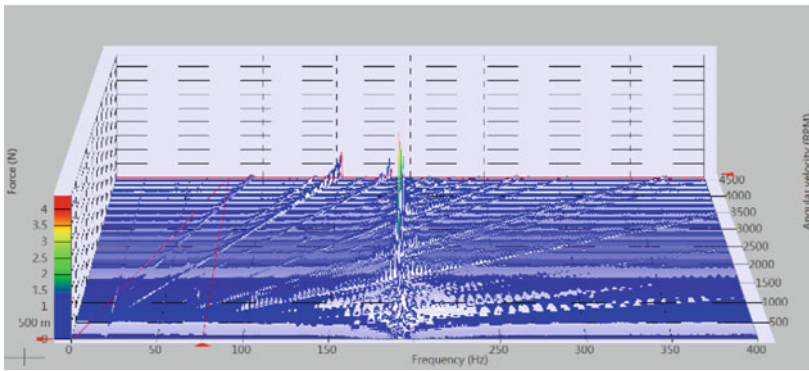
From Fig. 18, the characteristics of the micro-vibration are expressed as small magnitudes, all within 5 N; the frequency domain is wide. From the origin, there are multiple rays caused by harmonic excitation, and X- and Y-directions are more obvious than Z-direction, which is consistent with the theoretical model. There are three order natural modes within 400 Hz, which is the one-path mode of the wheel, the transverse mode and the local mode of the damper rings. The modal frequency is the same as the frequency of the previous test when the speed is 0. The first order has obvious forward and backward traveling waves, while the second-order traveling wave characteristics are not significant, and the third order has no traveling wave characteristics, which is consistent with the inherent characteristics of the simulation. When the frequency of the harmonic excitation is equal to the natural frequency of the rotation (intersection point), the vibration response takes a peak, and when the intersection point is a point on the forward wave, the amplitude of the intersection point is larger than the point peak on the backward wave, which is consistent with the simulation response characteristic of harmonic-wave excitation. Only the transverse mode can be clearly identified in Z-direction, indicating that the damper rings can absorb the energy of the other two modes in Z-direction.



(a) X direction



(b) Y direction



(c) Z direction

Fig. 18 The vibration output of the base output in three directions

5 Conclusions and Outlook

For the momentum wheel structural system, the micro-vibration characteristics are studied through theory, simulation and experiment. And the excitation model under the action of rotation is established. The conclusions are as followings:

- (1) The rim-spokes geometry of the wheel structure has the characteristics of non-uniform distribution of mass and stiffness. The local deformation of the rim will generate the traveling wave under the action of rotation. The asymmetric deformation on both ends of the strut structure will cause the time-varying stiffness of the bearings. These all constitute the parameter excitations of the system.
- (2) The wheel structure inevitably has unbalanced amounts, causing excitation at the same frequency as the rotating speed; after the rolling action of the bearing rollers, the (secondary) harmonic excitation will be formed, which together act as the load excitations of the system.
- (3) Establish a finite element model under the action of rotating, and obtain the characteristics of harmonic-wave excitation by harmonic response analysis; then verify the traveling wave characteristics by transient response analysis.
- (4) Test the inherent characteristics and response characteristics of the momentum wheel structural system, verify the correctness of the theoretical model and simulation calculation, including the mode shape and frequency caused by structural features, the harmonic excitation from the bearing support structure, and the traveling wave from the local vibration of the rim.

In the simulation of transient characteristic calculation, only the fundamental frequency is considered. And the high frequency can be taken into count in further research. The micro-vibration characteristics analysis based on the combination of intrinsic characteristics and response characteristics proposed in this paper is beneficial to the subsequent targeted suppression of the momentum wheel vibration problems.

References

1. Pang SW, Yang L, Qu GQ (2007) New development of micro-vibration integrated modeling and assessment technology for high performance spacecraft. *Struct Environ Eng* 06:1–9 (in Chinese)
2. Hasha MD (1986) Reaction wheel mechanical noise vibrations. Space Telescope Program, Engineering Memorandum, SSS-218
3. Masterson RA (1999) Development and validation of empirical and analytical reaction wheel disturbance models. Massachusetts Institute of Technology, Cambridge
4. Liu KC, Maghami P, Blaurock C (2008) Reaction wheel disturbance modeling, jitter analysis, and validation tests for solar dynamics observatory: AIAA-2008-7232. AIAA, Reston
5. Yang XF, Bai ZG, Yang D et al (2015) Study on micro-vibration of satellite induced by momentum wheels and on-orbit simulation analysis. *Equip Environ Eng* 12(03):15–21 + 41 (in Chinese)

6. Levine MB (1998) Interferometry program flight experiments. IPEX I and II, SPIE
7. Zhou WY (2012) Research on dynamic modeling and vibration control for the flywheel of spacecraft. National University of Defense Technology, Changsha, pp 35–39 (in Chinese)
8. Luo RZ, Zhang JY, Li LF et al (2017) Mechanism of micro-vibration excited by bearing rolling face geometrical errors. *J Vib Eng* 30(6):1066–1073 (in Chinese)
9. Li LJ, Dai JH (2005) Inner disturbance modeling and simulation analysis of reaction wheel system. *J Syst Simul* 17(8):1855–1858 (in Chinese)
10. Yan LT, Zhu ZG, Li QH et al (1994) High-speed rotating machinery vibration. National Defense Industry Publishing, Beijing (in Chinese)
11. Luo Q (2014) Research on micro-vibration characteristic and isolation methods of spacecraft flywheel system. National University of Defense Technology, Changsha, pp 8–10 (in Chinese)
12. Harris TA, Kotzalas MN (2009) Analysis of rolling bearings, 5th ed: Volume 1, Basic concept of bearing technology (Luo JW, Ma W et al, translated). Mechanical Industry Press, Beijing, pp 27–37 (in Chinese)
13. Zhao Y, Zhang PF, Cheng W (2009) Measure and study of disturbance characteristic of reaction wheel assembly. *J Exp Mech* 24(6):532–538 (in Chinese)
14. Ma YH, Liu SS, Wang H et al. Micro-vibration mechanism and simulation study of momentum wheel. *J Beijing Univ Aeronaut Astronaut* 1–10 [2019-04-27]. <https://doi.org/10.13700/j.bh.1001-5965.2018.0608> (in Chinese)
15. Wang ML (2013) Dynamics and vibration characteristics of misaligned rotor systems. Northeastern University (in Chinese)
16. Luo RZ, Hu G, Wang QW (2014) Radial vibration characteristics of a high-speed rotor of a cantilevered SGCMG. *J Vib Shock* 33(05):200–204